nature chemistry

ARTICLES

https://doi.org/10.1038/s41557-022-00954-9

Check for updates

Mechanism-based ligand design for copper-catalysed enantioconvergent C(sp^3)–C(sp) cross-coupling of tertiary electrophiles with alkynes

Fu-Li Wang[1,4], Chang-Jiang Yang[1,4], Ji-Ren Liu[2,4], Ning-Yuan Yang[1], Xiao-Yang Dong[1], Ruo-Qi Jiang[1], Xiao-Yong Chang[1], Zhong-Liang Li[3], Guo-Xiong Xu[2], Dai-Lei Yuan[1], Yu-Shuai Zhang[1], Qiang-Shuai Gu[3]✉, Xin Hong[2]✉ and Xin-Yuan Liu[1]✉

In contrast with the well-established enantioconvergent radical C(sp^3)–C cross-coupling of racemic secondary alkyl electrophiles, the corresponding coupling of tertiary electrophiles to forge all-carbon quaternary stereocentres remains underexplored. The major challenge arises from the steric hindrance and the difficult enantio-differentiation of three distinct carbon substituents of prochiral tertiary radicals. Here we demonstrate a general copper-catalysed enantioconvergent C(sp^3)–C(sp) cross-coupling of diverse racemic tertiary alkyl halides with terminal alkynes (87 examples). Key to the success is the rational design of chiral anionic *N,N,N*-ligands tailor-made for the computationally predicted outer-sphere radical group transfer pathway. This protocol provides a practical platform for the construction of chiral C(sp^3)–C($sp/sp^2/sp^3$) bonds, allowing for expedient access to an array of synthetically challenging quaternary carbon building blocks of interest in organic synthesis and related areas.

Transition metal-catalysed C–C cross-coupling reactions have revolutionized organic synthesis, providing an essential toolkit for the expedited synthesis of medicines, agrochemicals and functional material molecules[1–3]. With the goal of providing sustainable strategies for the synthesis of enantio-enriched three-dimensional (3D) molecules, great efforts have been dedicated to the development of chiral earth-abundant first-row transition metal catalysts (Ni, Co and Fe), which easily convert racemic alkyl electrophiles to prochiral alkyl radicals via a single-electron transfer (SET) process[4–7]. Accordingly, the enantioconvergent C(sp^3)–C cross-coupling of racemic secondary (2°) alkyl electrophiles has been established with these catalysts (Fig. 1a, left)[4–7]. However, tertiary (3°) alkyl electrophiles have rarely been accommodated in this kind of coupling reaction for the construction of sterically congested all-carbon quaternary stereocentres[8,9], which would otherwise provide an excellent complementary approach to the established asymmetric transformations of tertiary alkyl electrophiles via a heterolytic C–X cleavage strategy[10–22]. This is primarily because of the steric hindrance of corresponding tertiary radicals and the difficulty in the enantio-differentiation of its three different carbon substituents[10,11]. In an important advance, the enantioconvergent radical C(sp^3)–C(sp^2/sp^3) cross-coupling of racemic tertiary alkyl halides under nickel/bisoxazoline catalysis has recently been accomplished (Fig. 1a, right)[8,9]. Despite these efforts, the mechanism for the reactions between the highly reactive tertiary radicals and the chiral metal catalysts has so far remained unclear, let alone the origins of the stereochemical control, thereby posing substantial hurdles for the development of more general methods.

To address these abovementioned challenges and to take advantage of copper catalysis[23–25], we initially tried our recently developed anionic *N,N,P*-ligand/Cu catalysts[26–28] for coupling racemic secondary alkyl halides (Fig. 1b) in the coupling reaction of a racemic α-aminocarbonyl-α-phenyl alkyl chloride with phenylacetylene. Unfortunately, all attempts met with only marginal enantioselectivity, although good yield was generally observed (≤11% e.e., ≤73% yield, Supplementary Fig. 1). Preliminary density functional theory (DFT) calculations revealed that the coupling of the tertiary alkyl radical and alkynyl group proceeded preferably via an outer-sphere radical substitution-type C–C bond-formation pathway (Supplementary Fig. 11 and Supplementary Table 6). This is in stark contrast with that of the secondary alkyl radical, which was proposed to involve the reductive elimination from an inner-sphere Cu(III) intermediate formed upon radical trapping[26,29] (Fig. 1c, left). Apparently, the enantio-determining transition states in the outer-sphere C–C bond-formation mechanism (Fig. 1c, right) are more loosely organized, with effective enantio-discriminating interactions[30] probably occurring farther away from the first coordination spheres around the copper centres, compared with their counterparts with the inner-sphere C–C bond-formation mechanism (Fig. 1c, left). As such, we envisaged that a rationally redesigned ligand scaffold with tailor-made features was necessary to achieve enantiocontrol of the outer-sphere radical group transfer pathway (Fig. 1d): (1) low steric congestion immediately around the first coordination sphere for facile accommodation of sterically bulky tertiary alkyl radicals and (2) a long spreading side arm to competently interact[30] with either or both substrates in the outer side of the second coordination sphere for efficient stereodiscrimination.

To this end, in this Article we describe our efforts in developing a set of amide-derived anionic *N,N,N*-ligands for realizing a general copper-catalysed enantioconvergent radical C(sp^3)–C(sp)

[1]Shenzhen Grubbs Institute and Department of Chemistry, Guangdong Provincial Key Laboratory of Catalysis, Southern University of Science and Technology, Shenzhen, China. [2]Center of Chemistry for Frontier Technologies, Department of Chemistry, Zhejiang University, Hangzhou, China. [3]Academy for Advanced Interdisciplinary Studies and Department of Chemistry, Southern University of Science and Technology, Shenzhen, China. [4]These authors contributed equally: Fu-Li Wang, Chang-Jiang Yang, Ji-Ren Liu. ✉e-mail: guqs@sustech.edu.cn; hxchem@zju.edu.cn; liuxy3@sustech.edu.cn

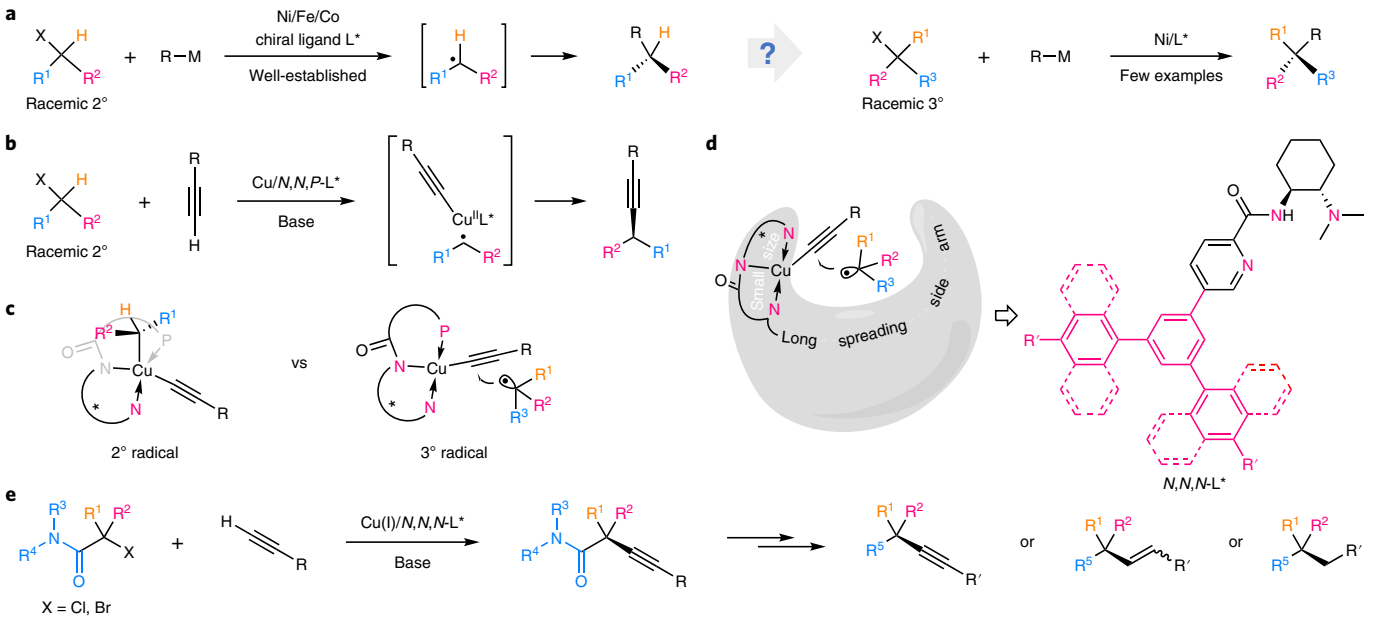

Fig. 1 | Motivation and design of Cu-catalysed enantioconvergent cross-coupling of racemic tertiary alkyl halides with terminal alkynes. a, The transition metal-catalysed enantioconvergent radical C(sp^3)–C cross-coupling of racemic secondary alkyl halides has been well-established, whereas that with racemic tertiary alkyl halides has hitherto remained underdeveloped due to the challenges associated with the great steric hindrance, the difficult enantio-differentiation of the tertiary radical, and the unclear stereocontrol model. **b**, Our previous work on C(sp^3)–C(sp) cross-coupling of racemic secondary alkyl halides with Cu(I)/*N,N,P*-ligand catalysts[26]. **c**, Different radical coupling mechanisms for secondary and tertiary alkyl radicals. For the 2° radical, inner-sphere pathway, compact transition state, interactions more close to Cu. For the 3° radical, outer-sphere pathway, loose transition state, interactions more distant to Cu. **d**, Rational design of chiral ligands for the enantiocontrol of coupling with tertiary alkyl radicals. **e**, This work on enantioconvergent radical C(sp^3)–C(sp) coupling of racemic tertiary alkyl halides with terminal alkynes. Eighty-seven examples; up to 90% yield, up to 95% e.e.

cross-coupling of racemic tertiary alkyl halides with terminal alkynes under mild reaction conditions. The reaction features broad substrate scopes (87 examples) with respect to both coupling partners, covering diverse tertiary α-aminocarbonyl alkyl chlorides and bromides and a variety of (hetero)aryl-, alkenyl- and alkyl-substituted terminal alkynes with good functional group compatibility and excellent enantioselectivity (Fig. 1e). More importantly, this strategy provides universal access to an abundance of compounds possessing distinct substitution types of quaternary carbon stereocentres when allied with follow-up transformations, thus providing a complementary approach to the enantioconvergent cross-coupling of tertiary electrophiles with organometallics.

Results and discussion

Ligand design and reaction development. To introduce the envisioned side arm, at the outset we tried to replace the phosphine moiety in previous *N,N,P*-ligands[26–28,31] with a common pyridine ring, considering its multiple substitutable C–H bonds with well-defined directions as well as its relatively small steric bulkiness. The thus modified *N,N,N*-ligand **L*1**[32] (Table 1) successfully afforded the coupling product **1** from the reaction of racemic tertiary alkyl chloride **E1** and phenylacetylene **A1** in 65% yield, albeit with still low enantioselectivity (41% e.e.), thus demonstrating the competence of the *N,N,N*-coordination manifold for promoting the desired reaction. Further replacing the key chiral skeleton with other popular diamines resulted in only slight improvement of the enantioselectivity (**L*2**–**L*5**), indicating the general lack of competent stereodiscriminating elements among these ligands. Accordingly, we next sought to install the conceived side arm for achieving effective enantiocontrol. To our delight, ligand **L*6** bearing a *meta*-phenyl substituent on the pyridyl group delivered obviously enhanced enantioselectivity (72% e.e.). Changing the arm to the bulkier 1-naphthyl (**L*7**) and 9-anthryl (**L*8**) groups further improved the enantioselectivity to around 80% e.e. This salient improvement trend prompted us to investigate sterically even larger 3,5-disubstituted phenyl rings (**L*9**–**L*11**) and the e.e. increased to 86% using **L*11**. The enantioselectivity enhancement was not strictly dependent on the chosen chiral skeleton, as the same sterically bulky side arm in **L*12** also provided greatly improved enantiocontrol in comparison with that of **L*3**. These results collectively indicated the presence of essential stereodiscriminating interactions in the distant region away from the copper centre as well as the backbones of the diamines. In accord with our aforementioned conjecture, increasing the steric congestion close to the first coordination sphere, either by introducing an *ortho*-methyl group on the pyridyl ring (**13**) or by changing the *N,N*-dimethyl amino group to bulkier piperidinyl (**14**) and *N,N*-dibenzyl amino (**15**) groups, inevitably led to greatly diminished reaction efficiency and enantioselectivity. These observations probably resulted from new interactions between the substrates and the ligands that came into play immediately around the first coordination sphere, disfavouring the radical attack and disrupting the enantio-discrimination process. Further evaluation of other reaction parameters led to the discovery of the optimal reaction conditions as follows: the reaction of **E1** (1.0 equiv.) and **A1** (1.5 equiv.) in the presence of $Cu(OTf)_2$ (10 mol%), **L*11** (15 mol%) and Cs_2CO_3 (3.0 equiv.) afforded **1** in 73% yield with 91% e.e. in the mixed solvent of methyl *tert*-butyl ether (MTBE)/cyclohexane (vol/vol = 2/3) at 10 °C (Table 2; for details of the reaction optimization, see Supplementary Table 1). In addition, the large-scale reaction of **E1** and **A1** performed under the same reaction conditions gave the desired chiral alkyne **1** with almost the same yield and e.e. (Table 2).

Substrate scope. With the optimal conditions in hand, we examined the generality of this enantioconvergent C(sp^3)–C(sp) coupling reaction (Table 2). With regard to the scope of α-aminocarbonyl-α-aryl alkyl halides, a range of secondary amides derived from aniline and

Table 1 | The design of ligands in the model reaction

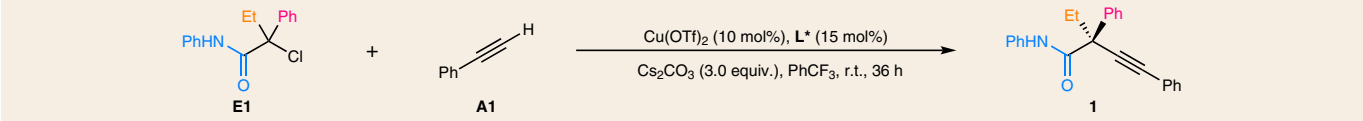

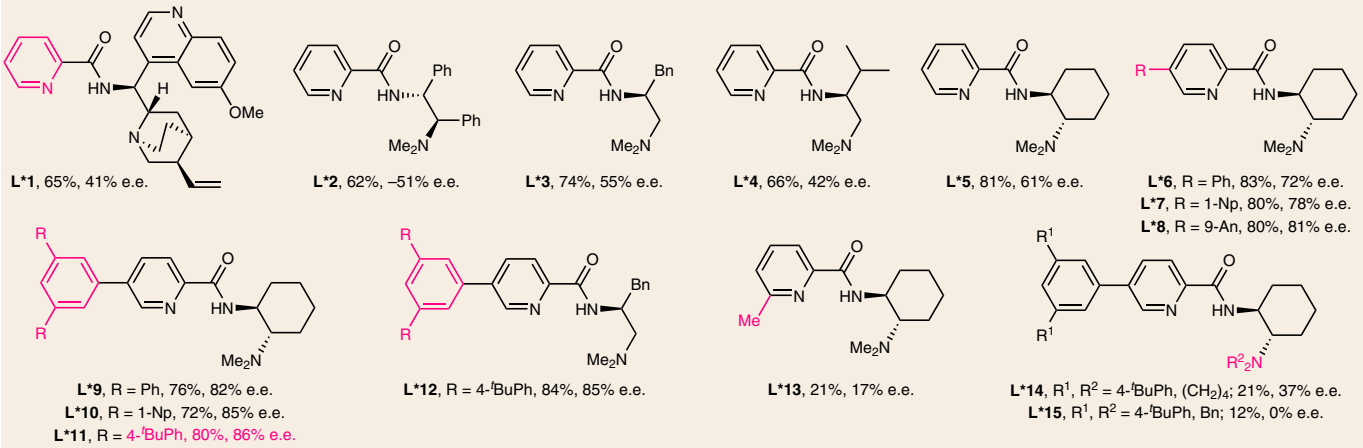

Reaction conditions: **E1** (0.025 mmol, 1.0 equiv.), **A1** (1.5 equiv.), $Cu(OTf)_2$ (10 mol%), **L*** (15 mol%) and Cs_2CO_3 (3.0 equiv.) in dry $PhCF_3$ (0.50 ml) at room temperature (r.t.) for 36 h under argon. Yield is based on ^{1}H-NMR analysis of the crude product using 1,3,5-trimethoxybenzene as an internal standard. The e.e. of **1** is based on HPLC analysis. Np, naphthalenyl; An, anthryl; ^{t}Bu, *tert*-butyl.

its analogues were suitable substrates to provide the corresponding products **1**–**11** in up to 82% yield with 86–94% e.e. (for results for other α-aryl alkyl halides, see Supplementary Figs. 2 and 3). As for the α-substituents, many substrates bearing simple unfunctionalized aliphatic side chains or those functionalized with terminal phenyl, trifluoromethyl, ether, chloro and olefin groups were all well accommodated in this process to deliver **12**–**18** in 62–83% yields with 86–93% e.e. In addition, a panel of α-phenyl rings with electron-donating or -withdrawing groups at different positions as well as an α-naphthyl ring were compatible with the reaction conditions, affording **19**–**28** with 80–94% e.e. In terms of the scope of alkyne substrates, a variety of substituted aryl alkynes all worked well to give **29**–**44** in moderate to good yields with excellent e.e. A gamut of functional groups, such as halo (**29**–**33**), formyl (**39**), ester (**40**), nitrile (**41**) and olefin (**42**), were well tolerated under the standard conditions. Furthermore, many heteroaryl alkynes containing medicinally relevant heterocycles such as thiophene (**45** and **46**), benzo[*b*]thiophene (**47**), benzo[*b*]furan (**48**), pyridine (**49**), quinoline (**50**) and even a ferrocene-derived alkyne (**51**) were viable substrates, providing products with excellent e.e. More importantly, a number of alkenyl and alkyl alkynes underwent the reaction smoothly to generate **52**–**61** with 83–94% e.e. It is noteworthy that many functional groups, such as conjugating alkene (**53** and **54**), cyclopropane (**55**), nitrile (**56**), acetal (**57**), ester (**58**), ether (**59**), carbazole (**60**) and thioether (**61**), were left untouched.

Encouraged by the above success, we went on to investigate the reaction of α,α-dialkyl-substituted electrophiles (Table 3), during which the enantio-differentiation of two alkyl groups is necessary and more difficult[33]. As expected, the original optimal ligand **L*11** exhibited only marginal enantiocontrol (31% e.e.; Supplementary Fig. 4) for one alkyl bromide of this kind under standard conditions, and the corresponding alkyl chloride proved to be unreactive. Consistent with our notion regarding the abovementioned ligand design, further increasing the steric bulkiness of the side arm together with other minor condition modifications quickly restored the high enantioselectivity (Supplementary Table 2). Accordingly, various (hetero)aryl and alkenyl alkynes were successfully coupled with a set of α,α-dialkyl-substituted alkyl bromides to give **62**–**69** with moderate to excellent enantioselectivity under the reoptimized conditions (Table 3). It is noteworthy that the reaction on the most challenging α-ethyl-α-methyl-substituted alkyl bromide delivered product **70** in promising enantioselectivity; this is currently under further optimization in our laboratory.

To further strengthen the synthetic potential of this methodology, we next investigated the coupling of 2-azetidinone-derived tertiary alkyl bromides with alkynes (Table 4), given the importance of enantio-enriched β-lactams as key motifs in natural products and active pharmaceutical ingredients[34–37] as well as valuable synthons in organic synthesis[38]. Interestingly, the desired product **71** was directly obtained from the corresponding coupling partners with 75% yield and 73% e.e. (Supplementary Table 3) in the presence of simple *N*,*N*,*N*-ligand **L*1** (Table 1). By contrast, **L*5** (Table 1), having the best chiral diamine backbone for acyclic tertiary halide substrates, only delivered marginal enantioselectivity (28% e.e., Supplementary Table 3) for the cyclic bromide. These results probably indicate enantio-determining transition states with the azetidinone-derived alkyl radical residing closer to the copper centre due to its relatively small bulkiness. In this case, interactions closer to the first coordination sphere might become important for effective enantio-discrimination. After additional systematic optimization of reaction parameters (Supplementary Table 3), we identified **L*17**–**19** as effective ligands for the coupling of various sorts of alkynes and 2-azetidinone-derived tertiary alkyl bromides (Table 4). Most importantly, the reaction on bromide substrates bearing secondary α-alkyl groups or even an α-ethyl group provided products **85**–**87** with good yield and excellent enantioselectivity, thus largely overcoming the enantio-differentiation issue with the α,α-dialkyl substituents for this coupling methodology. The absolute configurations of **44** (Table 2 and Supplementary Fig. 7), **55** (Table 2 and Supplementary Fig. 8) and **79** (Table 4 and Supplementary Fig. 9) were determined to be *S* by X-ray crystallographic analysis, and all other compounds were assigned by analogy accordingly.

Synthetic utility. To demonstrate the synthetic potential of this strategy (Fig. 2a), we readily converted the alkyne moiety in the enantio-enriched product **1** to an alkyl group in **88** or *E*-/*Z*-alkenyl groups in **89**/**90**, respectively, in one reduction step. In addition, we transformed the amide motif in **1** to an amine group in **91**, an

Table 2 | Substrate scopes of α-aminocarbonyl-α-aryl alkyl chlorides and alkynes

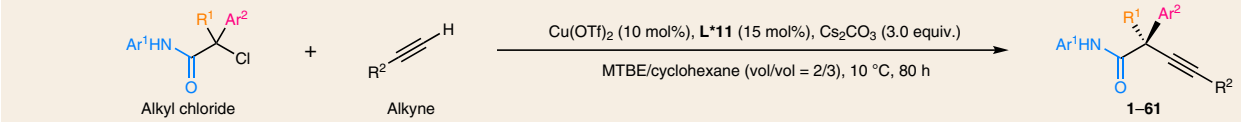

Scope of Ar^1 in alkyl chlorides

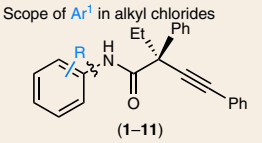

(**1**–**11**)

H, **1**, 73%, 91% e.e.
70%, 91% e.e. for large scale[a]

p-OMe, **2**
54%, 91% e.e.[b]

p-^{t}Bu, **3**
52%, 92% e.e.

p-Ph, **4**
63%, 91% e.e.

p-Br, **5**
46%, 92% e.e.

p-CF_3, **6**
39%, 94% e.e.

m-F, **7**
39%, 94% e.e.

3,5-Me_2, **8**
63%, 91% e.e.

3,5-OMe_2, **9**
43%, 93% e.e.

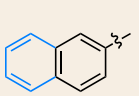

10, 74%, 86% e.e.

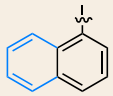

11, 82% , 93% e.e.

Scope of R^1 in alkyl chlorides

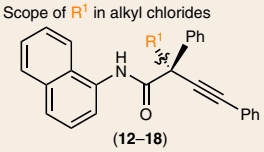

(**12**–**18**)

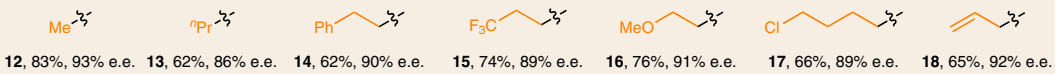

12, 83%, 93% e.e. **13**, 62%, 86% e.e. **14**, 62%, 90% e.e. **15**, 74%, 89% e.e. **16**, 76%, 91% e.e. **17**, 66%, 89% e.e. **18**, 65%, 92% e.e.

Scope of Ar^2 in alkyl chlorides

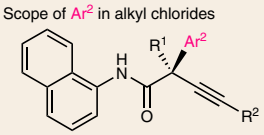

(**19**, **20**, **26**, R^1 = Me, R^2 = PCP)
(**21**, **23**, R^1 = Et, R^2 = Ph)
(**22**, **25**, **27**, **28**, R^1 = Me, R^2 = Ph)
(**24**, R^1 = Et, R^2 = PCP)

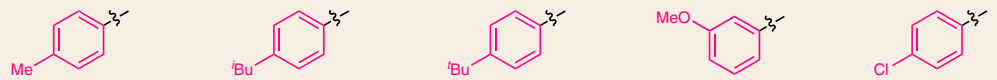

19, 63%, 94% e.e. **20**, 53%, 91% e.e. **21**, 68%, 82% e.e. **22**, 48%, 94% e.e. **23**, 55%, 87% e.e.

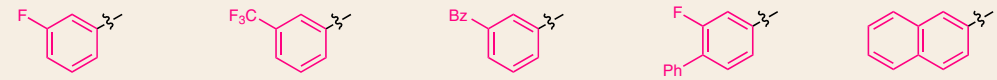

24, 57%, 89% e.e. **25**, 74%, 80% e.e. **26**, 51%, 88% e.e. **27**, 53%, 88% e.e. **28**, 57%, 82% e.e.

Scope of R^2 in (hetero)aryl alkynes

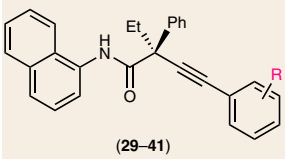

(**29**–**41**)

p-Cl, **29**
78%, 94% e.e.

m-Cl, **30**
65%, 92% e.e.

o-Cl, **31**
53%, 91% e.e.

p-F, **32**
75%, 93% e.e.

p-Br, **33**
86%, 94% e.e.

p-OMe, **34**
84%, 91% e.e.

m-OMe, **35**
68%, 93% e.e.

p-Me, **36**
63%, 95% e.e.

p-Et, **37**
82%, 90% e.e.

p-Ph, **38**
77%, 93% e.e.

p-CHO, **39**
61%, 94% e.e.

p-CO_2Me, **40**
47%, 93% e.e.

p-CN, **41**
55%, 94% e.e.

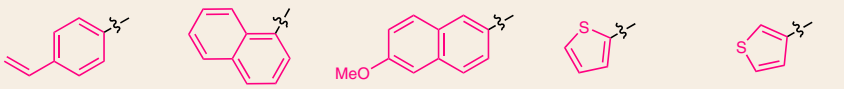

42, 72%, 92% e.e. **43**, 73%, 88% e.e. **44**, 81%, 90% e.e. **45**, 62%, 94% e.e. **46**, 86%, 94% e.e.

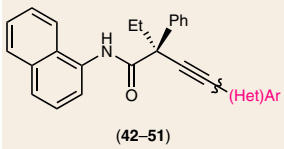

(**42**–**51**)

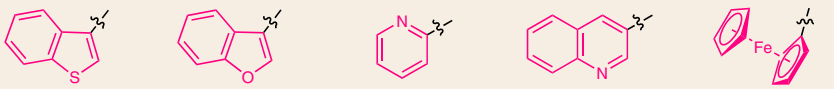

47, 76%, 90% e.e. **48**, 61%, 92% e.e. **49**, 64%, 93% e.e.[c] **50**, 70%, 94% e.e. **51**, 90%, 91% e.e.[c]

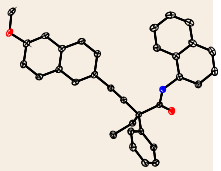

X-ray structure of **44**

Scope of R^2 in alkenyl and alkyl alkynes

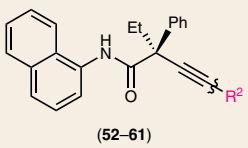

(**52**–**61**)

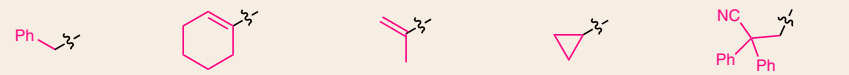

52
47%, 88% e.e.[c]

53
73%, 92% e.e.

54
68%, 92% e.e.[c]

55
51%, 89% e.e.[c]

56
63%, 90% e.e.[c]

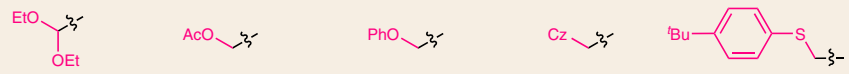

57
55%, 94% e.e.[c]

58
49%, 83% e.e.[c]

59
63%, 87% e.e.[c]

60
63%, 90% e.e.[c]

61
51%, 90% e.e.[c]

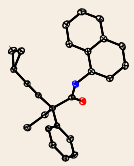

X-ray structure of **55**

Standard conditions: racemic alkyl chloride (0.10 mmol), alkyne (1.5 equiv.), $Cu(OTf)_2$ (10 mol%), **L*11** (15 mol%) and Cs_2CO_3 (3.0 equiv.) in MTBE/cyclohexane (vol/vol = 2/3, 2.0 ml) under argon at 10 °C for 80 h. Isolated yields are shown. [a]**E1** (2.0 mmol) was used. [b]A mixture of CF_3Ph/cyclohexane (vol/vol = 2/3, 2.0 ml) was used as solvent. [c]**L*12** (15 mol%). PCP, *para*-cyanophenyl; Cz, 9-carbazolyl.

alcohol group in **92**, an aldehyde group in **93**, an ester group in **94** and a carboxylic acid group in **95** in one or two steps. Hence, the combination of the current C(sp^3)–C(sp) coupling method with appropriate following manipulations well complements the direct cross-coupling approaches for a diverse variety of tertiary alkyl electrophiles with alkyl or alkenyl nucleophiles. Moreover, we chemoselectively converted the alkyne and amide functionalities in **1** to a range of other common functional groups, including the 1,4-ketoester in **96**, γ-lactone in **97** and γ-lactam in **98**, in one or two steps. Further hydrogenation of **98** led to the formation of a new stereocentre in **99** in moderate diastereoselectivity. It is noteworthy that no apparent loss of enantiopurity was observed during all these transformations, demonstrating the practicability of the synthetic strategy in the expedient access of diverse enantio-enriched building blocks with all-carbon quaternary stereocentres.

Mechanistic considerations. We first synthesized complex **C1** of **L*7** with Cu(II), on which the X-ray structural analysis clearly indicated an anionic tridentate coordination mode of the ligand (Fig. 2b and Supplementary Fig. 10). Further control experiments

Table 3 | Substrate scopes of α-dialkyl-substituted alkyl bromides and alkynes

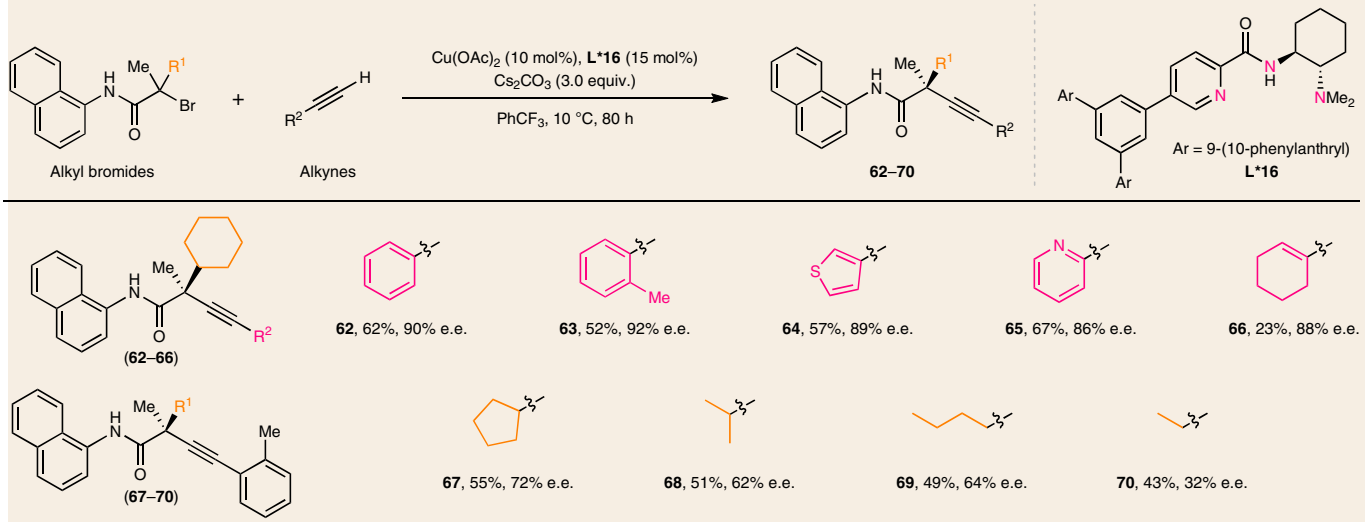

Standard conditions: racemic alkyl bromide (0.10 mmol), alkyne (1.5 equiv.), Cu(OAc)$_2$ (10 mol%), **L*16** (15 mol%) and Cs_2CO_3 (3.0 equiv.) in $PhCF_3$ (2.0 ml) under argon at 10 °C for 80 h. Isolated yields are shown.

Table 4 | Substrate scopes of 2-azetidinone-derived alkyl bromides and alkynes

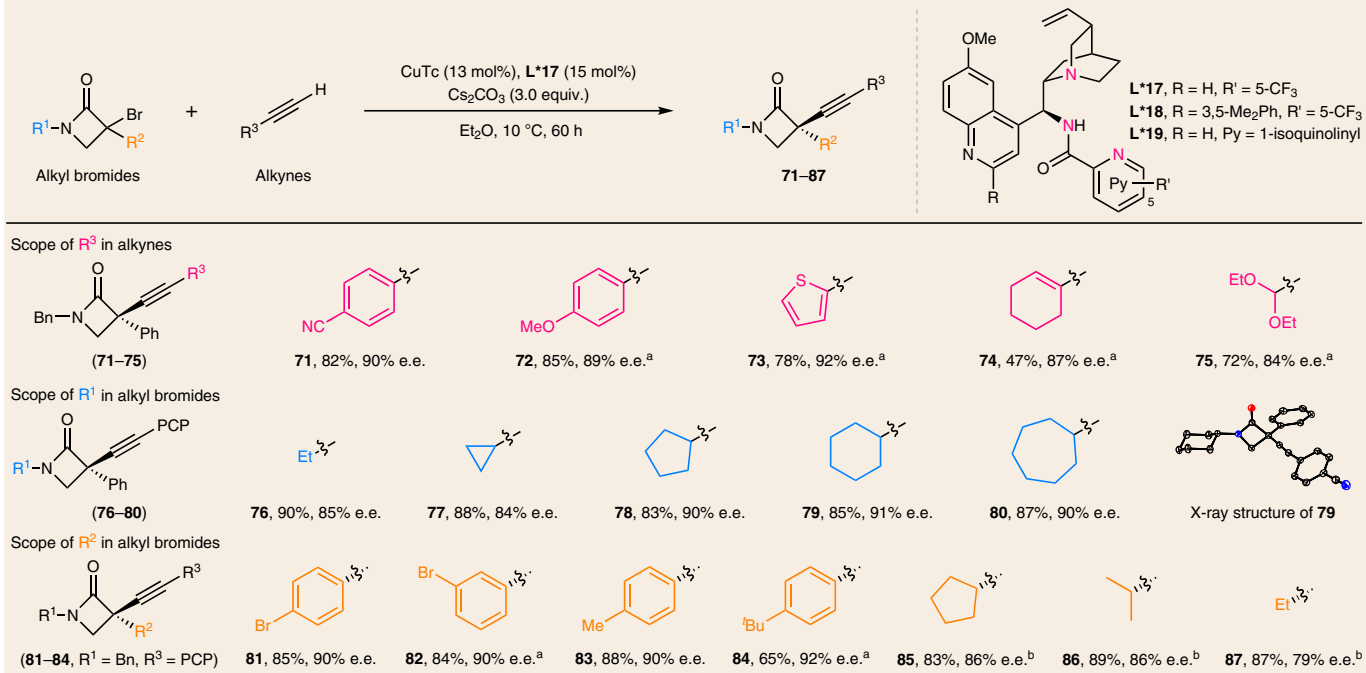

Standard conditions: racemic alkyl bromide (0.10 mmol), alkyne (1.2 equiv.), CuTc (13 mol%), **L*17** (15 mol%) and Cs_2CO_3 (3.0 equiv.) in dry Et_2O (2.0 ml) at 10 °C for 60 h under argon. Isolated yields are shown. [a]**L*18** (15 mol%) was used. [b]3-(*N*-carbazoly)propyne (1.2 equiv.), **L*19** (15 mol%) and dry $PhCF_3$ (2.0 ml) were used at 40 °C for 64 h under argon.

revealed that complex **C1** and the in situ generated catalyst from Cu(OTf)$_2$ and **L*7** afforded similar enantioselectivity under the otherwise identical reaction conditions (Fig. 2c). We also observed a linear relationship between the enantiopurities of the products and the corresponding ligands, suggesting the involvement of one single chiral ligand in the enantio-determining transition state (Fig. 2d). These observations together supported a monomeric copper species tridentately coordinated by the *N*,*N*,*N*-ligand as the active catalyst in this process. Second, the reaction of stoichiometric copper acetylide **A1′** with **E2** provided the coupling product **11** in comparable enantioselectivity with that of the reaction between **A1** and **E2** under standard conditions (Fig. 2e). However, both reactions failed to produce **11** in the absence of **L*11** under otherwise the same conditions. Thus, the ligand-coordinated copper acetylide might serve as the key species for the reaction initiation and product formation. Third, no apparent enantio-enrichment of the recovered alkyl chloride **E2** was observed in the reactions under typical conditions (Fig. 2f), disfavouring a possible kinetic resolution

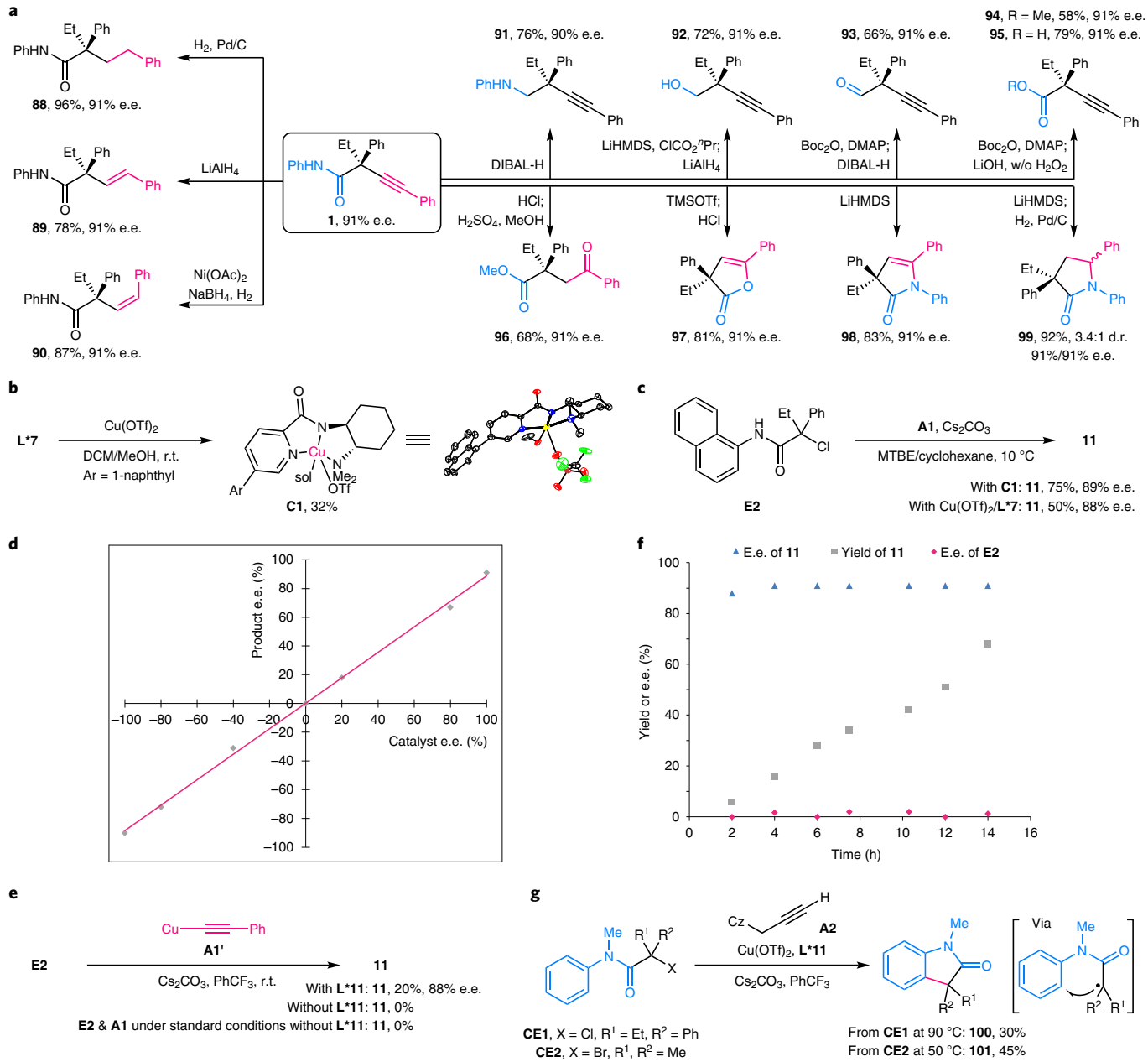

Fig. 2 | Synthetic utility and mechanistic discussion. a, The alkyne and amide motifs in the enantio-enriched product **1** could be readily converted to other common and useful functional groups either individually (**88**–**90** and **91**–**95**) or together (**96**–**99**) in one or two steps, without any loss of enantiopurity, providing facile access to a diverse range of valuable chiral building blocks featuring all-carbon quaternary stereocentres (see the synthetic application section in the Supplementary Information for detailed conditions). **b**, Synthesis and X-ray structure of the **L***Cu complex **C1**. **c**, The use of complex **C1** or its synthetic precursors $Cu(OTf)_2$ and **L*7** as catalyst led to comparable reaction efficiency and enantioselectivity under the otherwise standard conditions, indicating common catalytically active species involved in these two reactions. **d**, The nonlinear effect study revealed a linear relationship between the enantiopurities of the products and the corresponding ligands, favouring a 1:1 Cu-to-ligand ratio in the enantio-determining step. **e**, Control experiments indicated the indispensable role of the ligand-coordinated copper acetylide in the reaction initiation and product formation. **f**, No apparent kinetic resolution of the alkyl chloride was observed and the nearly constant product enantiopurity favoured a uniform mechanism throughout the reaction. **g**, Radical clock experiments indicating the formation of tertiary alkyl radical intermediates. DIBAL-H, diisobutylaluminium hydride; LiHMDS, lithium bis(trimethylsilyl)amide; TMS, trimethylsilyl; OTf, triflate; sol, methanol.

of **E2**. Moreover, the observed product e.e. values at different time intervals remained nearly constant, favouring the involvement of a uniform mechanism throughout the reaction course. In addition, the radical clock substrates **CE1** and **CE2** gave rise to the corresponding cyclization products **100** and **101**, respectively, under the typical conditions, arguing for the formation of corresponding tertiary alkyl radical intermediates (Fig. 2g). All in all, these results are in agreement with a working mechanism involving the initial single-electron reduction of the alkyl halides to prochiral radicals by ligand-coordinated copper acetylide followed by enantioselective radical $C(sp^3)$–$C(sp)$ coupling[39,40].

We next performed DFT calculations to understand the reaction mechanism and the origins of enantioselectivity. The DFT-computed free energy changes of the operative catalytic cycle

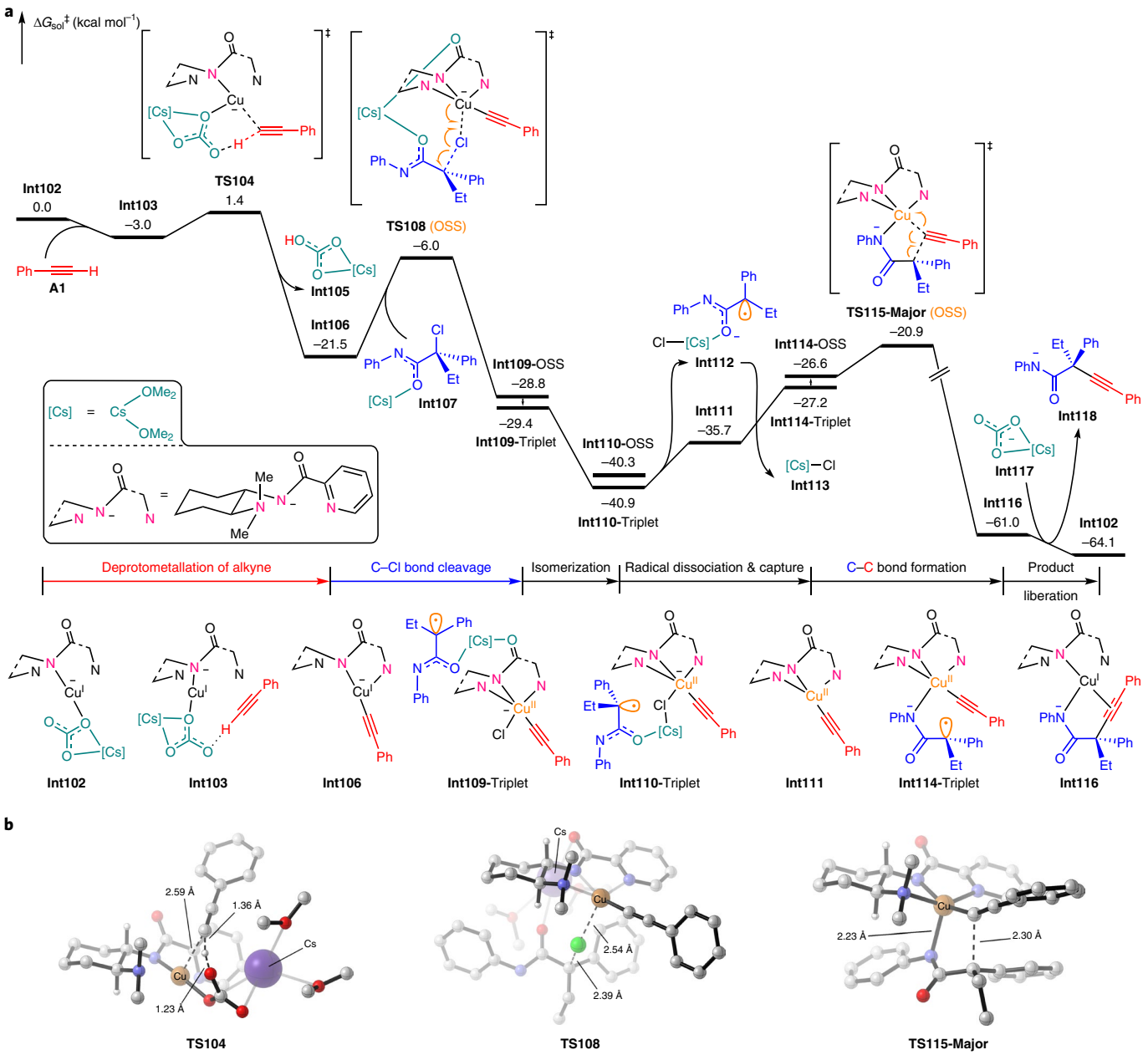

Fig. 3 | Model DFT study on the operative catalytic cycle. a, DFT-computed free energy changes of the operative catalytic cycle with the model ligand **L*5** at B3LYP-D3(BJ)/6-311+G(d,p)-SDD-SMD(Cyclohexane)// B3LYP-D3(BJ)/6-31G(d)-LANL2DZ level of theory. The catalytical cycle involves the deprotonation of alkyne **A1**, C–Cl bond cleavage of radical precursor **Int107**, isomerization of triplet diradical species **Int109**-Triplet, radical dissociation and capture from **Int110**-Triplet to **Int114**-Triplet, copper-mediated C–C bond formation of diradical intermediate **Int114**-Triplet, and product liberation. **b**, 3D structures of key alkyne deprotonation transition state **TS104**, C–Cl bond cleavage transition state **TS108**, and copper-mediated C–C bond-formation transition state **TS115-Major**.

are shown in Fig. 3, and more details are provided in Supplementary Table 6 and the computational studies section in the Supplementary Information. Using **L*5** as a truncated model, we first examined the generation of the active Cu(I) catalyst from the Cu(II) precatalyst **L*5**Cu^{II}OTf (**C1-Model**). Starting from this precatalyst, sequential alkynylation and dinuclear alkynyl–alkynyl reductive elimination lead to the energetically stable active LCu(I) catalyst **Int102** (Supplementary Figs. 12 and 13; for details see the computational studies section in the Supplementary Information). **Int102** first complexes with alkyne **A1** to form **Int103**, which then undergoes a facile deprotonation of ethynylbenzene via **TS104** to generate the alkynylated Cu(I) intermediate **Int106**. This facile deprotonation was also confirmed in the neutral model involving Cs_2CO_3 (Supplementary Fig. 14). We believe that the amide N–H of the alkyl halide is deprotonated under basic conditions, based on the NMR analysis (Supplementary Figs. 5 and 6; for details, see the mechanistic studies section in the Supplementary Information). Thus, subsequent C–Cl bond cleavage of the deprotonated radical precursor **Int107** occurs through the chlorine atom transfer transition state **TS108**, leading to the triplet diradical species **Int109**-Triplet. Alternative pathways for the C–Cl bond cleavage (oxidative addition, dissociative electron transfer and stepwise outer-sphere electron transfer) were also explored[41–43], and the details are included in the computational studies section and Supplementary Figs. 15–19

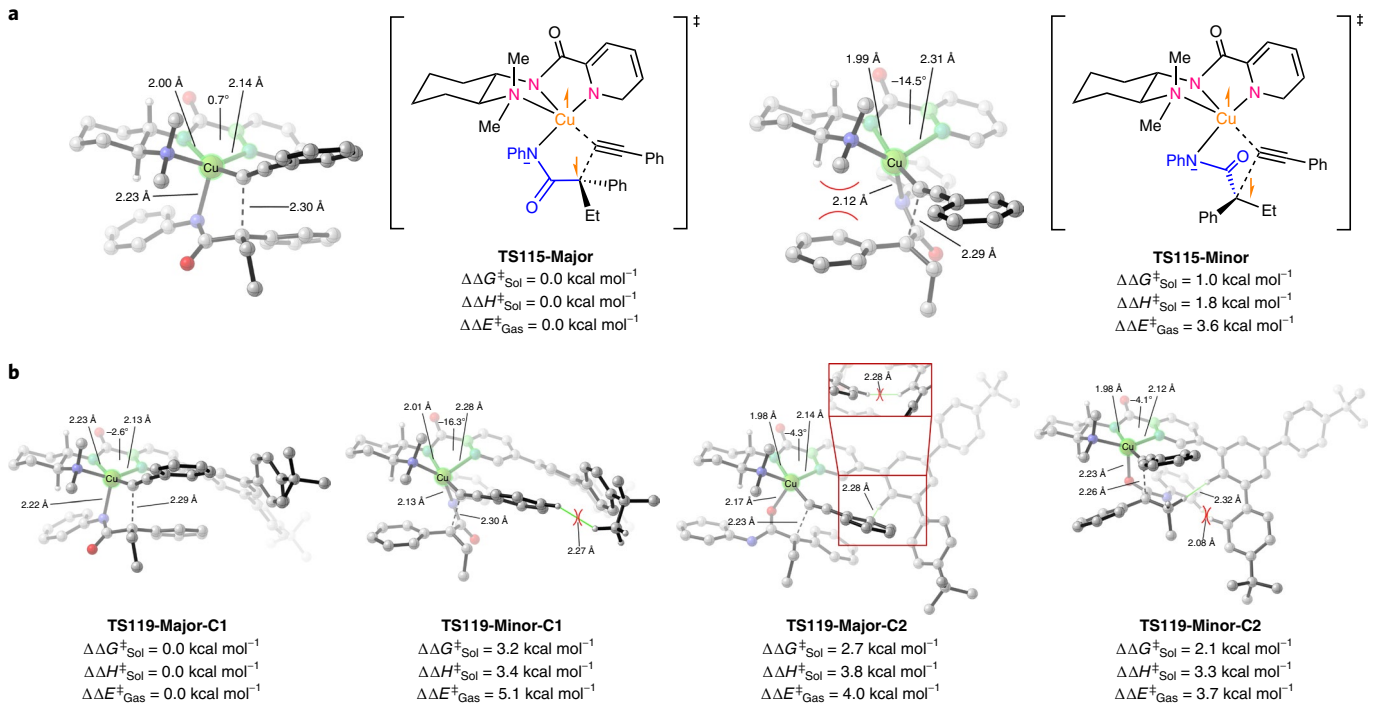

Fig. 4 | DFT calculations on enantioselectivity control. a, Optimized structures and relative energies of the enantioselectivity-determining C–C bond-formation transition states using the truncated model ligand **L*5** without the bulky side arm. The moderate enantioselectivity of **L*5** is due to the highlighted steric repulsion in **TS115-Minor** between the *N*–Me substituent of the ligand and the α-phenyl group of the tertiary radical species. **b**, Optimized structures and relative energies of the enantioselectivity-determining C–C bond-formation transition states using the optimal ligand **L*11** with bulky side arm. The side arm of ligand **L*11** disfavours both conformations of the minor C–C bond-formation transition states **TS119-Minor-C1** and **TS119-Minor-C2** due to the highlighted additional steric repulsions, which improves the enantioselectivity of the C–C bond-formation process. The suffix 'C1' refers to a *N*-binding mode of the alkyl radical to copper with one of the bulky 4-^{t}BuPh moieties protruding from the upper right section of the drawn structure. The suffix 'C2' refers to an *O*-binding mode of the alkyl radical to copper with one of the bulky 4-^{t}BuPh moieties protruding from the lower right section of the drawn structure.

in the Supplementary Information. From **Int109**-Triplet, the radical-caesium fragment dissociates from the ligand carbonyl group and binds to the copper-coordinating chlorine, generating the more stable intermediate **Int110**-Triplet. **Int110**-Triplet liberates **Int112**, the complex of the alkyl radical and caesium chloride, leading to the LCu^{II}(alkynyl) intermediate **Int111**. Next, the radical is captured by **Int111**, releasing caesium chloride and generating the diradical intermediate **Int114**. **Int114** has both triplet and open-shell singlet (OSS) states. The triplet state **Int114**-Triplet is more stable than **Int114**-OSS by 0.6 kcal mol^{-1}. However, the triplet C–C bond-formation transition state **TS115**-Triplet is 3.5 kcal mol^{-1} less favourable than the open-shell singlet transition state **TS115-Major** (Supplementary Fig. 21). Therefore, the C–C bond formation proceeds via the open-shell singlet radical substitution-type transition state **TS115-Major**, which irreversibly creates the quaternary stereogenetic centre in **Int116**. **Int116** eventually liberates the cross-coupling product and regenerates the Cu(I) active catalyst **Int102**. For the C–C bond-formation process, we also considered alternative pathways including sequential SET and carbocation bonding as well as the Cu(III)–Cu(I) reductive elimination. Both pathways are less favourable compared to the radical substitution-type pathway via **TS115-Major** (Supplementary Figs. 20–22; more details on the C–C bond-formation mechanism are included in the computational studies section in the Supplementary Information). Based on the DFT calculations of the catalytic cycle, the irreversible radical substitution-type C–C bond formation determines the enantioselectivity of cross-coupling.

Comparisons of the enantioselectivity-determining transition states between the reactions involving **L*5** (without a side arm) and **L*11** (with a pendant bulky side arm) elucidated the origins of enantio-induction by the bulky side arm (Fig. 4; for details of extensive conformational searches, see Supplementary Figs. 24–31 and Supplementary Tables 4–7). The enantioisomeric C–C bond-formation transition states **TS115-Major** and **TS115-Minor** with **L*5** only have a 1.0 kcal mol^{-1} free energy difference, favouring the (*S*)-product (Fig. 4a). This is consistent with the observed moderate enantioselectivity (61% e.e., 0.8 kcal mol^{-1} ΔΔ*G*, Table 1). The major reason for the differentiation is the highlighted steric repulsion between one of the *N*–Me substituents in the ligand and the α-phenyl group of the radical species. Such a steric repulsion is limited due to the small-sized methyl substitution. With the installation of an additional bulky side arm (**L*11**), our computations identified the enhancement of enantio-differentiation. The key transition states **TS119-Major-C1/-C2** and **TS119-Minor-C1/-C2** with **L*11** are elaborated in Fig. 4b; 'C1' and 'C2' here refer to the *N*-coordinating and *O*-coordinating configurations of the alkyl radical, respectively. The introduction of the bulky side arm leads to additional steric repulsions with the radical species or alkynyl fragments in both the minor (**TS119-Minor-C1** and **TS119-Minor-C2**) and one major (**TS119-Major-C2**) C–C bond-formation transition state. Only in **TS119-Major-C1** does the side arm not lead to considerable extra steric repulsions. The geometry of **TS115-Major** with **L*5** is very close to that of the corresponding fragment in **TS119-Major-C1** (root-mean-square deviation (r.m.s.d.) = 0.0182 Å; Supplementary Fig. 23). This emphasizes the enantio-differentiation by the additional side arm in the C–C bond-formation process, which results in a 2.1 kcal mol^{-1} free energy difference between the major and minor C–C bond-formation pathways and improved enantioselectivity (**TS119-Major-C1** versus **TS119-Minor-C2**).

Conclusion

In summary, we have established a robust strategy for Cu-catalysed enantioconvergent radical C(sp^3)–C(sp) coupling of diverse racemic tertiary electrophiles with terminal alkynes under mild conditions. The key to success is the rational design of anionic *N*,*N*,*N*-ligands featuring low steric congestion immediately around the coordination atoms for ready accommodation of sterically bulky tertiary radicals and a long spreading side arm for efficient enantio-discrimination on the basis of the calculated enantio-determining outer-sphere radical group transfer pathway. Further straightforward transformations of the coupling products in one or two steps quickly generated a library of useful compounds characterized by over ten distinct types of functional group with up to two stereocentres, thus showcasing the potential of this strategy for the expedient assembly of diverse synthetically challenging enantio-enriched quaternary carbon building blocks. We anticipate that this strategy will soon spur more efforts in ligand and catalyst design for developing more asymmetric cross-coupling reactions of sterically congested tertiary alkyl radicals derived from diverse readily available precursors with different types of nucleophile.

Online content

Any methods, additional references, Nature Research reporting summaries, source data, extended data, supplementary information, acknowledgements, peer review information; details of author contributions and competing interests; and statements of data and code availability are available at https://doi.org/10.1038/s41557-022-00954-9.

Received: 8 May 2021; Accepted: 21 April 2022;
Published online: 26 May 2022

References

1. Johansson Seechurn, C. C. C., Kitching, M. O., Colacot, T. J. & Snieckus, V. Palladium-catalyzed cross-coupling: a historical contextual perspective to the 2010 Nobel Prize. *Angew. Chem. Int. Ed.* **51**, 5062–5085 (2012).
2. de Meijere, A., Bräse, S. & Oestreich, M. (eds) *Metal-Catalyzed Cross-Coupling Reactions and More* (Wiley, 2014).
3. Biffis, A., Centomo, P., Del Zotto, A. & Zecca, M. Pd metal catalysts for cross-couplings and related reactions in the 21st century: a critical review. *Chem. Rev.* **118**, 2249–2295 (2018).
4. Choi, J. & Fu, G. C. Transition metal-catalyzed alkyl-alkyl bond formation: another dimension in cross-coupling chemistry. *Science* **356**, eaaf7230 (2017).
5. Fu, G. C. Transition-metal catalysis of nucleophilic substitution reactions: a radical alternative to S_N1 and S_N2 processes. *ACS Cent. Sci.* **3**, 692–700 (2017).
6. Cherney, A. H., Kadunce, N. T. & Reisman, S. E. Enantioselective and enantiospecific transition-metal-catalyzed cross-coupling reactions of organometallic reagents to construct C-C bonds. *Chem. Rev.* **115**, 9587–9652 (2015).
7. Bullock, R. M. et al. Using nature's blueprint to expand catalysis with Earth-abundant metals. *Science* **369**, eabc3183 (2020).
8. Wang, Z., Yin, H. & Fu, G. C. Catalytic enantioconvergent coupling of secondary and tertiary electrophiles with olefins. *Nature* **563**, 379–383 (2018).
9. Wang, Z., Yang, Z.-P. & Fu, G. C. Quaternary stereocentres via catalytic enantioconvergent nucleophilic substitution reactions of tertiary alkyl halides. *Nat. Chem.* **13**, 236–242 (2021).
10. Quasdorf, K. W. & Overman, L. E. Catalytic enantioselective synthesis of quaternary carbon stereocentres. *Nature* **516**, 181–191 (2014).
11. Liu, Y., Han, S.-J., Liu, W.-B. & Stoltz, B. M. Catalytic enantioselective construction of quaternary stereocenters: assembly of key building blocks for the synthesis of biologically active molecules. *Acc. Chem. Res.* **48**, 740–751 (2015).
12. Wu, L., Yang, G. & Zhang, W. Ni-catalyzed enantioconvergent coupling of epoxides with alkenylboronic acids: construction of oxindoles bearing quaternary carbons. *CCS Chem.* **2**, 623–631 (2020).
13. Trost, B. M. & Jiang, C. Atom economic asymmetric creation of quaternary carbon: regio- and enantioselective reactions of a vinylepoxide with a carbon nucleophile. *J. Am. Chem. Soc.* **123**, 12907–12908 (2001).
14. Zhang, P., Le, H., Kyne, R. E. & Morken, J. P. Enantioselective construction of all-carbon quaternary centers by branch-selective Pd-catalyzed allyl–allyl cross-coupling. *J. Am. Chem. Soc.* **133**, 9716–9719 (2011).
15. Ma, S., Han, X., Krishnan, S., Virgil, S. C. & Stoltz, B. M. Catalytic enantioselective stereoablative alkylation of 3-halooxindoles: facile access to oxindoles with C3 all-carbon quaternary stereocenters. *Angew. Chem. Int. Ed.* **48**, 8037–8041 (2009).
16. Tsuchida, K., Senda, Y., Nakajima, K. & Nishibayashi, Y. Construction of chiral tri- and tetra-arylmethanes bearing quaternary carbon centers: copper-catalyzed enantioselective propargylation of indoles with propargylic esters. *Angew. Chem. Int. Ed.* **55**, 9728–9732 (2016).
17. Zhao, W., Wang, Z., Chu, B. & Sun, J. Enantioselective formation of all-carbon quaternary stereocenters from indoles and tertiary alcohols bearing a directing group. *Angew. Chem. Int. Ed.* **54**, 1910–1913 (2015).
18. Li, X. et al. Catalytic enantioselective synthesis of chiral tetraarylmethanes. *Nat. Catal.* **3**, 1010–1019 (2020).
19. Wendlandt, A. E., Vangal, P. & Jacobsen, E. N. Quaternary stereocentres via an enantioconvergent catalytic S_N1 reaction. *Nature* **556**, 447–451 (2018).
20. Zhang, X. et al. An enantioconvergent halogenophilic nucleophilic substitution (S_N2X) reaction. *Science* **363**, 400–404 (2019).
21. Li, J. et al. Formal enantioconvergent substitution of alkyl halides via catalytic asymmetric photoredox radical coupling. *Nat. Commun.* **9**, 2445 (2018).
22. Murakata, M., Jono, T., Mizuno, Y. & Hoshino, O. Construction of chiral quaternary carbon centers by catalytic enantioselective radical-mediated allylation of α-iodolactones using allyltributyltin in the presence of a chiral Lewis acid. *J. Am. Chem. Soc.* **119**, 11713–11714 (1997).
23. Evano, G. & Blanchard, N. (eds) *Copper-Mediated Cross-Coupling Reactions* (Wiley, 2014).
24. Chemler, S. R. Copper's contribution to amination catalysis. *Science* **341**, 624–626 (2013).
25. Gu, Q.-S., Li, Z.-L. & Liu, X.-Y. Copper(I)-catalyzed asymmetric reactions involving radicals. *Acc. Chem. Res.* **53**, 170–181 (2020).
26. Dong, X.-Y. et al. A general asymmetric copper-catalysed Sonogashira C(sp^3)–C(sp) coupling. *Nat. Chem.* **11**, 1158–1166 (2019).
27. Jiang, S.-P. et al. Copper-catalyzed enantioconvergent radical Suzuki-Miyaura C(sp^3)-C(sp^2) cross-coupling. *J. Am. Chem. Soc.* **142**, 19652–19659 (2020).
28. Su, X.-L. et al. Copper-catalyzed enantioconvergent cross-coupling of racemic alkyl bromides with azole C(sp^2)–H bonds. *Angew. Chem. Int. Ed.* **60**, 380–384 (2021).
29. Dong, X.-Y. et al. Copper-catalyzed asymmetric radical 1,2-carboalkynylation of alkenes with alkyl halides and terminal alkynes. *J. Am. Chem. Soc.* **142**, 9501–9509 (2020).
30. Proctor, R. S. J., Colgan, A. C. & Phipps, R. J. Exploiting attractive non-covalent interactions for the enantioselective catalysis of reactions involving radical intermediates. *Nat. Chem.* **12**, 990–1004 (2020).
31. Sladojevich, F., Trabocchi, A., Guarna, A. & Dixon, D. J. A new family of cinchona-derived amino phosphine precatalysts: application to the highly enantio- and diastereoselective silver-catalyzed isocyanoacetate aldol reaction. *J. Am. Chem. Soc.* **133**, 1710–1713 (2011).
32. Hayashi, M., Shiomi, N., Funahashi, Y. & Nakamura, S. Cinchona alkaloid amides/dialkylzinc catalyzed enantioselective desymmetrization of aziridines with phosphites. *J. Am. Chem. Soc.* **134**, 19366–19369 (2012).
33. Zhang, F.-H., Zhang, F.-J., Li, M.-L., Xie, J.-H. & Zhou, Q.-L. Enantioselective hydrogenation of dialkyl ketones. *Nat. Catal.* **3**, 621–627 (2020).
34. Banik, B. K. (ed.) *β-Lactams*: *Unique Structures of Distinction for Novel Molecules* (Springer, 2013).
35. Decuyper, L. et al. Antibacterial and β-lactamase inhibitory activity of monocyclic β-lactams. *Med. Res. Rev.* **38**, 426–503 (2018).
36. Galletti, P. & Giacomini, D. Monocyclic β-lactams: new structures for new biological activities. *Curr. Med. Chem.* **18**, 4265–4283 (2011).
37. Pitts, C. R. & Lectka, T. Chemical synthesis of β-lactams: asymmetric catalysis and other recent advances. *Chem. Rev.* **114**, 7930–7953 (2014).
38. Ojima, I., Zuniga, E. S. & Seitz, J. D. in *β-Lactams*: *Unique Structures of Distinction for Novel Molecules* (ed. Banik, B. K.) 1–64 (Springer, 2013).
39. Wu, L., Wang, F., Chen, P. & Liu, G. Enantioselective construction of quaternary all-carbon centers via copper-catalyzed arylation of tertiary carbon-centered radicals. *J. Am. Chem. Soc.* **141**, 1887–1892 (2019).
40. Kainz, Q. M. et al. Asymmetric copper-catalyzed C-N cross-couplings induced by visible light. *Science* **351**, 681–684 (2016).
41. Lin, C. Y., Coote, M. L., Gennaro, A. & Matyjaszewski, K. Ab initio evaluation of the thermodynamic and electrochemical properties of alkyl halides and radicals and their mechanistic implications for atom transfer radical polymerization. *J. Am. Chem. Soc.* **130**, 12762–12774 (2008).
42. Isse, A. A., Bortolamei, N., De Paoli, P. & Gennaro, A. On the mechanism of activation of copper-catalyzed atom transfer radical polymerization. *Electrochim. Acta* **110**, 655–662 (2013).
43. Fang, C. et al. Mechanistically guided predictive models for ligand and initiator effects in copper-catalyzed atom transfer radical polymerization (Cu-ATRP). *J. Am. Chem. Soc.* **141**, 7486–7497 (2019).

Methods

Synthesis of 1–61. Under an argon atmosphere, an oven-dried resealable Schlenk tube equipped with a magnetic stirring bar was charged with $Cu(OTf)_2$ (3.6 mg, 0.010 mmol, 10 mol%), **L*11** or **L*12** (0.015 mmol, 15 mol%), Cs_2CO_3 (98.0 mg, 0.30 mmol, 3.0 equiv.) and a mixed solvent of MTBE and cyclohexane (vol/vol = 2/3, 2.0 ml). Then, alkyl halide (0.10 mmol, 1.0 equiv.) and alkyne (0.15 mmol, 1.5 equiv.) were sequentially added into the mixture and the reaction mixture was stirred at 10 °C for 80 h. On completion, the precipitate was filtered off and washed with CH_2Cl_2. The combined filtrate was evaporated and the residue was purified by column chromatography on silica gel to afford the desired products **1**–**61**.

Synthesis of 62–70. Under an argon atmosphere, an oven-dried resealable Schlenk tube equipped with a magnetic stirring bar was charged with $Cu(OAc)_2$ (1.8 mg, 0.010 mmol, 10 mol%), **L*16** (12.4 mg, 0.015 mmol, 15 mol%), Cs_2CO_3 (98.0 mg, 0.30 mmol, 3.0 equiv.) and CF_3Ph (2.0 ml). Then, alkyl halide (0.10 mmol, 1.0 equiv.) and alkyne (0.15 mmol, 1.5 equiv.) were sequentially added into the mixture and the reaction mixture was stirred at 10 °C for 80 h. On completion, the precipitate was filtered off and washed with CH_2Cl_2. The combined filtrate was evaporated and the residue was purified by column chromatography on silica gel to afford the desired products **62**–**70**.

Synthesis of 71–84. Under an argon atmosphere, an oven-dried resealable Schlenk tube equipped with a magnetic stirring bar was charged with CuTc (2.5 mg, 0.013 mmol, 10 mol%), **L*17** or **L*18** (0.015 mmol, 15 mol%), Cs_2CO_3 (98.0 mg, 0.30 mmol, 3.0 equiv.) and Et_2O (2.0 ml). Then, alkyl halide (0.10 mmol, 1.0 equiv.) and alkyne (0.12 mmol, 1.2 equiv.) were sequentially added into the mixture and the reaction mixture was stirred at 10 °C for 60 h. On completion, the precipitate was filtered off and washed with CH_2Cl_2. The combined filtrate was evaporated and the residue was purified by column chromatography on silica gel to afford the desired products **71**–**84**.

Synthesis of 85–87. Under an argon atmosphere, an oven-dried resealable Schlenk tube equipped with a magnetic stirring bar was charged with CuTc (2.5 mg, 0.013 mmol, 10 mol%), **L*19** (7.2 mg, 0.015 mmol, 15 mol%), Cs_2CO_3 (98.0 mg, 0.30 mmol, 3.0 equiv.) and CF_3Ph (2.0 ml). Then, alkyl halide (0.10 mmol, 1.0 equiv.) and alkyne (0.12 mmol, 1.2 equiv.) were sequentially added into the mixture and the reaction mixture was stirred at 40 °C for 64 h. On completion, the mixture was allowed to cool to room temperature and the precipitate was filtered off and washed with CH_2Cl_2. The combined filtrate was evaporated and the residue was purified by column chromatography on silica gel to afford the desired products **85**–**87**.

Data availability

Data relating to the materials and methods, optimization studies, experimental procedures, mechanistic studies, DFT calculations, HPLC spectra, NMR spectra and mass spectrometry are available in the Supplementary Information. Crystallographic data for the structures reported in this Article have been deposited at the Cambridge Crystallographic Data Centre, under deposition nos. CCDC 2074298 (**44**), 2074300 (**55**), 2074301 (**79**) and 2074302 (**C1**). Copies of the data can be obtained free of charge via https://www.ccdc.cam.ac.uk/structures/.

Acknowledgements

We thank the National Natural Science Foundation of China (grants nos. 21831002 and 22025103 to X.-Y.L., 21901106 to F.-L.W., 22001109 to Q.-S.G. and 21702182, 21873081 and 22122109 to X.H.), Guangdong Innovative Program (no. 2019BT02Y335 to X.-Y.L.), Guangdong Provincial Key Laboratory of Catalysis (no. 2020B121201002 to X.-Y.L.), Shenzhen Special Funds (no. JCYJ20200109141001789 to X.-Y.L.), SUSTech Special Fund for the Construction of High-Level Universities (no. G02216303 to X.-Y.L.), Fundamental Research Funds for the Central Universities (no. 2020XZZX002-02 to X.H.), the Starry Night Science Fund of Zhejiang University Shanghai Institute for Advanced Study (no. SN-ZJU-SIAS-006 to X.H.), the State Key Laboratory of Clean Energy Utilization (no. ZJUCEU2020007 to X.H.) and Key Laboratory of Precise Synthesis of Functional Molecules of Zhejiang Province (no. PSFM2021-01 to X.H.) for financial support. We appreciate the assistance of SUSTech Core Research Facilities with compound characterization. We also appreciate the support of the Center of Chemistry for Frontier Technologies, Department of Chemistry, Zhejiang University. Calculations were performed on the high-performance computing system at the Department of Chemistry, Zhejiang University.

Author contributions

X.-Y.L. and Q.-S.G. conceived and supervised the project. F.-L.W., C.-J.Y., N.-Y.Y., X.-Y.D., R.-Q.J., X.-Y.C., Z.-L.L., D.-L.Y. and Y.-S.Z. designed and performed the experiments and analysed the data. X.H. designed the DFT calculations. J.-R.L. and G.-X.X. performed the DFT calculations. X.-Y.L., X.H. and Q.-S.G. wrote the manuscript. All authors discussed the results and commented on the manuscript.

Competing interests

The authors declare no competing interests.

Additional information

Supplementary information The online version contains supplementary material available at https://doi.org/10.1038/s41557-022-00954-9.

Correspondence and requests for materials should be addressed to Qiang-Shuai Gu, Xin Hong or Xin-Yuan Liu.

Peer review information *Nature Chemistry* thanks the anonymous reviewer(s) for their contribution to the peer review of this work.